Smeared Impedance Model for Variable Depth Liners

Noah H. Schiller,[1] and Michael G. Jones[2]

NASA Langley Research Center, Hampton, VA 23681 USA

Noise from modern aircraft engines has a significant broadband component, which has motivated the need for broadband acoustic engine liners. A promising broadband design, called a variable depth liner, is composed of groups of resonators tuned for different frequencies. The accuracy of commonly used smeared impedance models, however, has not been thoroughly assessed for this type of liner. Therefore, the purpose of this study is to assess, and if necessary develop, semi-analytical impedance models for variable depth designs. The impedance prediction is complicated by the fact that the radiation loading on individual resonators within the array can be different. While the radiation loading can be neglected on conventional engine liners that consist of a dense array of uniform resonators, the same is not true for variable depth liners. To better understand and model this effect, nine liner samples are tested in the NASA Langley normal incidence tube. Comparisons of predicted and measured data for relatively simple non-uniform samples confirm that the radiation loading can be approximated using mass end correction terms. Semi-analytical impedance models that incorporate the proposed end corrections provide favorable comparisons with measured impedance spectra for variable depth liner samples.

I.   Introduction

CONVENTIONAL single-layer acoustic liners, which consist of a perforated facesheet over a honeycomb core, are often used in the engine nacelle to reduce fan noise. While this type of liner can be effective for tonal noise, modern high-bypass-ratio engines also have a significant broadband component. Therefore, more emphasis has been placed on broadband designs in recent years [1, 2]. A promising broadband design, called a variable depth liner, is composed of groups of resonators tuned for different frequencies. In this case, tuning is achieved by varying the depth of the backing cavity. When sets of resonators are grouped together into unit cells, and then replicated over the entire surface of the liner, the liner can be modeled using a uniform smeared impedance. This is an efficient representation of the liner, however the accuracy of commonly used smeared impedance models has not been thoroughly assessed for variable depth liners.

The purpose of this study is to assess, and if necessary develop, semi-analytical impedance models for variable depth liners. Accurate impedance models are needed to expedite the design and eliminate the need for an iterative build and test loop. In addition, accurate semi-analytical models are desirable for use in future optimization studies.

This paper begins with a description of nine liner samples, which include a standard uniform-depth array, several non-uniform samples, and two variable depth samples. In this context, non-uniform implies that the individual resonators are sparsely distributed in the sample. The test setup, consisting of a normal incidence tube, is briefly described. Next, the semi-analytical model is discussed, along with proposed mass end corrections to account for radiation loading. Radiation loading is shown to be particularly important when the samples are not uniform. A numerical model is then described, which is included for comparison purposes. Finally, predictions and measurements are compared to assess the accuracy of the proposed model.

II.   Experimental Assessment

Three different types of samples are considered: a uniform depth sample representative of a conventional engine liner, non-uniform samples used to systematically investigate radiation impedance effects, and variable depth samples

---

[1] Research Engineer, Structural Acoustics Branch, Research Directorate, AIAA Member.
[2] Senior Research Scientist, Structural Acoustics Branch, Research Directorate, AIAA Associate Fellow.

designed for broadband attenuation. The samples were 3-D printed using stereolithography and contain one or more square channels located in the 5 by 5 array depicted in Fig. 1. Each of the 25 potential resonator locations is uniquely labeled. The labels are referenced in Table 1, which provides relevant dimensions, along with the position and depth of the channels within each sample. Since the purpose of the study is to evaluate the accuracy of impedance models for variable depth samples, tests were performed without facesheets to avoid introducing unnecessary uncertainty associated with the transfer impedance of the facesheet. The nine samples used in the test are described next.

The first sample listed in Table 1 is the uniform depth array labeled UD. The sample contains 25 resonators that all have a uniform cross section of 0.375" by 0.375" and a constant cavity depth of 1.505". In addition to the geometric properties of the sample, Table 1 also includes the static temperature measured during the test. Temperature variations affect the speed of sound and therefore shift the reactance. Therefore, the predictions included in this paper account for the static temperature measured during the test, as listed in the table.

The next six samples are referred to as non-uniform samples because the resonators are localized, and not evenly distributed over the entire grid. All resonators in the set of non-uniform samples have a cross section of 0.35" by 0.35" and a depth of 1.75". The first non-uniform sample, labeled NU1, contains a single resonator centered in the middle of the array. The next sample, labeled NU2, has a single resonator along the right edge of the sample. The next two samples, labeled NU3 and NU4, contain resonators along the diagonal, at locations D24 and D15, respectively. Sample NU5 is a combination of NU1 and NU4, with one resonator in the center of the sample and one in the corner. The final sample is similar to NU5, however the two resonators have been shifted along the diagonal.
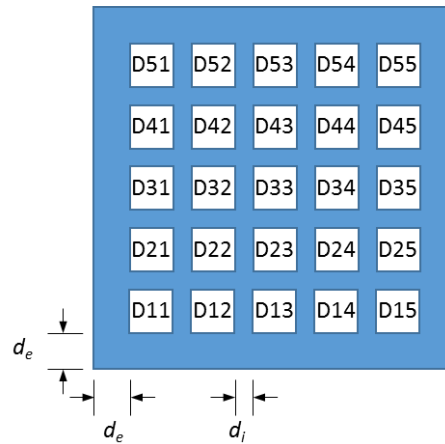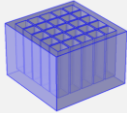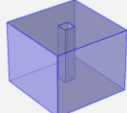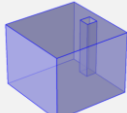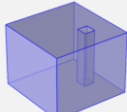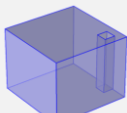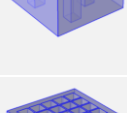

Fig. 1 Top view of a liner sample showing 25 potential resonator locations.

The final set of samples are referred to as variable depth liner samples. Each sample contains 25 resonators with a cross section of 0.375" by 0.375". The first sample in this set, labeled VD1, contains resonators with 7 unique depths ranging from 1.137" t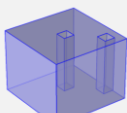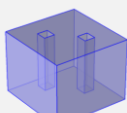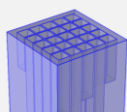o 3.386", with one-quarter wave resonance frequencies from approximately 1000 Hz to 3000 Hz. The second sample, labeled VD2, is similar, with 11 unique depths ranging from 1.132" to 3.386". In this case, the sample was designed to have equally spaced one-quarter wave resonance frequencies from approximately 1000 Hz to 3000 Hz in 200 Hz increments. It is important to note that both variable depth samples were arranged so that channels with the same depth are not adjacent to each other. The specific depth of each resonator, along with its relative location, are provided in Table 1.

Table 1 Description of the NIT samples.

Sample label	T_s [C]	d_e [in]	d_i [in]	Chamber cross-section [in]	Chamber depth(s) [in]	
Uniform Depth (UD)	23.3	0.213	0.050	0.375 x 0.375	(D11, D12, …, D55) = 1.505	
Non-Uniform (NU1)	21.5	0.25	0.0625	0.35 x 0.35	D33 = 1.75	
Non-Uniform (NU2)	21.8	0.25	0.0625	0.35 x 0.35	D35 = 1.75	
Non-Uniform (NU3)	22.0	0.25	0.0625	0.35 x 0.35	D24 = 1.75	
Non-Uniform (NU4)	22.9	0.25	0.0625	0.35 x 0.35	D15 = 1.75	
Non-Uniform (NU5)	23.3	0.25	0.0625	0.35 x 0.35	D33 = 1.75, D15 = 1.75	
Non-Uniform (NU6)	22.4	0.25	0.0625	0.35 x 0.35	D42 = 1.75, D24 = 1.75	
Variable Depth (VD1)	23.3	0.213	0.050	0.375 x 0.375	(D11, D12, …, D55) = 1.962, 3.386, 1.636, 2.823, 1.364, 2.353, 1.137, 1.962, 3.386, 1.636, 2.823, 1.364, 2.353, 1.137, 1.962, 3.386, 1.636, 2.823, 1.364, 2.353, 1.137, 1.962, 3.386, 1.636, 2.823	
Variable Depth (VD2)	23.0	0.213	0.050	0.375 x 0.375	(D11, D12, …, D55) = 1.883, 1.132, 2.420, 1.696, 3.386, 2.118, 1.542, 2.823, 1.883, 1.414, 2.420, 1.696, 1.305, 3.386, 1.542, 1.213, 2.823, 1.414, 1.132, 2.420, 1.305, 3.386, 2.118, 1.213, 2.823	

Measurements were acquired in the NASA Langley Normal Incidence Tube (NIT), depicted in Fig. 2. The impedance tube has a 2" x 2" cross section with acoustic drivers installed at one end of the tube, and the liner sample mounted at the other. A reference microphone located 0.25" from the surface of the liner sample is used to set the overall sound pressure level in the duct. All measurements presented in this paper were collected at a sound pressure level of 120 dB. Two additional microphones are installed 2.5" and 3.75" from the surface of the sample. The transfer-function method is used to calculate the impedance of the sample based on measurements from these microphones [3]. Specifically, the real and imaginary components of the normalized impedance are found versus frequency. The tests

described in this paper were performed using broadband noise from 400 Hz to 3000 Hz. The data was then processed to provide impedance in 25 Hz increments.
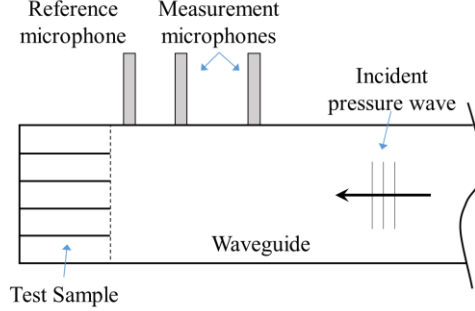

Fig. 2 Schematic of the NASA Langley Normal Incidence Tube (NIT).

III. Semi-Analytical Impedance Model

The resonators considered in this study are locally-reacting, which means there is no interaction between the resonators within the core. In addition, the cross-sectional dimensions of the resonators are small relative to the acoustic wavelength over the frequency range of interest. Therefore a one-dimensional plane-wave analysis can be used to derive the normalized specific acoustic input impedance for each cavity resonator as

$$\zeta_{cav} = -j\cot(k_c h) \tag{1}$$

where $j = \sqrt{-1}$, h is the depth of the cavity, and k_c is the complex-valued acoustic wavenumber, which captures thermal and viscous losses in the cavity. In this study, the Zwikker and Kosten low-reduced-frequency dissipation model, as described by Tijdeman, is used to define the cavity losses [4, 5]. Specifically, $k_c = -j\omega\Gamma/c$, where c is the ambient speed of sound, and Γ is the propagation constant defined as

$$\Gamma = \sqrt{\frac{J_0(j^{3/2}s)}{J_2(j^{3/2}s)}}\sqrt{\frac{\gamma}{n}} \tag{2}$$

In the previous expression, J_0 is the Bessel function of zero order, J_2 is the Bessel function of second order, $s = r\sqrt{\rho\omega/\mu}$ is the shear wave number, $r = \sqrt{A/\pi}$ is the effective radius of the channel, A is the cross-sectional area of the channel, ρ is the density of the gas, μ is the dynamic viscosity of the gas, and

$$n = \left(1 + \frac{\gamma-1}{\gamma}\frac{J_2(j^{3/2}s\sqrt{Pr})}{J_0(j^{3/2}s\sqrt{Pr})}\right)^{-1} \tag{3}$$

where γ is the ratio of heat capacities, and Pr is the Prandtl number. Note that $e^{j\omega t}$ time convention has been assumed in this paper.

In addition to the input impedance, the total impedance of a resonator also typically includes a mass end correction, which captures the radiation loading introduced by the external acoustic environment. The total normalized surface impedance for the resonator is therefore defined as

$$\zeta_t = \zeta_{cav} + j\chi_{rad} \tag{4}$$

where $k = \omega/c$ is the free-space wavenumber, $\chi_{rad} = k\delta$ is the radiation reactance, and δ is the mass end correction. The radiation reactance and mass end correction will be discussed in more detail in the following subsections.

Once the total impedance is determined for each resonator, the smeared surface impedance can be found by taking the reciprocal of the sum of the area averaged admittance of each resonator in the array. Specifically, the normalized surface admittance can be calculated for each resonator in the array as

$$\beta = 1/\zeta_t \tag{5}$$

The average admittance over the entire surface of the sample can then be calculated as

$$\beta_{avg} = \sum_{i=1}^{N} [\sigma_i \beta_i + (1 - \sigma_i)\beta_{hw}] \tag{6}$$

where σ_i is the ratio of the inlet area of the ith resonator to the total surface area of the sample, N is the total number of resonators in the array, and β_{hw} is the normalized equivalent surface admittance of the "hard-wall" portion of the liner. This parameter was set to zero for the predictions included in this paper. The smeared impedance can then be found as

$$\zeta_s = 1/\beta_{avg} \tag{7}$$

For uniform depth liner samples, the radiation reactance in Eq. (4) is negligible. The same is not true for variable-depth samples however. Therefore appropriate radiation reactance and mass end correction terms are needed for more general liner configurations. Before discussing mass end corrections, it is first helpful to review the concept of radiation impedance.

A. Radiation Impedance

Radiation impedance accounts for the effect of the external acoustic environment on the resonator. In general, it depends on the relative phase and amplitude of all other resonators in the array, as well as the location of external scattering surfaces. Typically, the resonator inlets are assumed to vibrate with a uniform velocity (i.e., as if they were a massless piston) and the radiation impedance is calculated as

$$z_n = z_{nn} + \sum_{m=1}^{N} \left(z_{nm}(v_m/v_n) \right) \tag{8}$$

where z_{nn} is the self-radiation impedance of the nth resonator (i.e., the radiation impedance of the resonator in isolation), z_{nm} is the mutual radiation impedance, which accounts for the induced pressure on the inlet of the nth resonator due to radiation from the mth resonator, and v_m/v_n is the ratio of inlet velocities [6]. In other words, the radiation impedance is a combination of the self-radiation impedance for an individual resonator and the sum of the mutual impedance (weighted by the ratio of inlet velocities) for all other resonators in the array. Recall that variable depth liners are composed of groups of resonators tuned for different frequencies. Since the mutual impedance is multiplied by the ratio of inlet velocities, and the inlet velocity of each resonator is only significant near resonance, then the interaction between resonators tuned for different frequencies will be neglected.

Additional assumptions are necessary to derive closed-form expressions for the self and mutual radiation impedance terms. Specifically, if the piston (representing the resonator inlet) is set in an infinite baffle, and $2kr \ll 1$, which is a low frequency assumption, then the self-radiation impedance can be approximated as

$$z_{nn} = \rho c \frac{(kr)^2}{2} + j\rho c \frac{8kr}{3\pi} \tag{9}$$

where $r = \sqrt{A/\pi}$ is the effective radius and A is the cross-sectional area of the piston [7]. Similarly, the mutual radiation impedance between two pistons in an infinite baffle can be approximated as

$$z_{nm} = \rho c \frac{(kr)^2}{2} \left(\frac{\sin(kd)}{kd} + j\frac{\cos(kd)}{kd} \right) \tag{10}$$

where d is the separation distance between the resonators [6]. Note that the radiation reactance, which is included in the total impedance expression in Eq. (4), is proportional to $\cos(kd)/(kd)$. This expression is plotted versus frequency in Fig. 3 for two different values of d. The first curve corresponds to adjacent resonators in one of the variable depth samples, $d = 0.425$", and the second curve corresponds to resonators separated by one position, $d = 0.85$". As expected, increasing the separation distance reduces the mutual impedance. The mutual interaction is therefore most important when resonators with the same natural frequency are located next to each other.
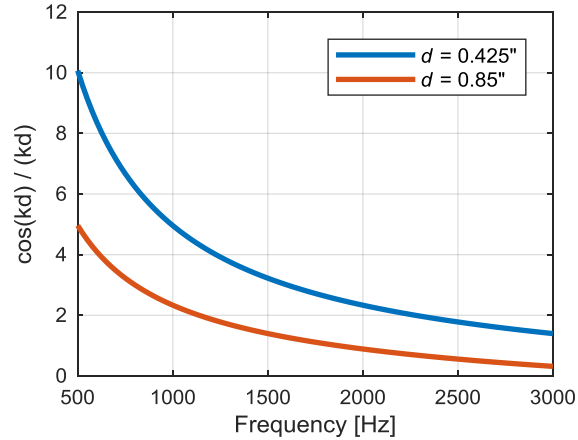
5

Fig. 3 Term proportional to the mutual radiation reactance between two pistons separated by _d_.

B. Equivalent Representation

The previous expressions for the self and mutual radiation impedance are helpful, but are not consistent with the current test results. Recall that the liner samples are tested in an impedance tube, not an infinite baffle, as the derivations for Eqs. (9) and (10) assumed. In other words, the resonators are radiating into a duct, not an infinite half space. To use these expressions to model samples installed in an impedance tube, it is helpful to reformulate the problem using the image source method, as discussed for instance in Ref. [7]. Specifically, the geometrical symmetry imposed by the rigid duct walls can be leveraged to create an equivalent 2D resonator array, as depicted in Fig. 4. The original sample, shown at the top, is mirrored and replicated to create the larger 2D array shown in the middle set of images. The images on the bottom show the smallest periodic unit cell that makes up the array. Using the equivalent representations shown in Fig. 4, the radiation impedance for arbitrary combinations of resonators can be estimated using Eqs. (8), (9), and (10). Assumptions are needed, however, to specify the ratio of inlet velocities. One option is to assume that the inlet velocities of resonators with the same depth are equal, while the inlet velocities of all other resonators in the array are zero. This assumption is not entirely accurate, but may be acceptable in some situations. Note that to be mathematically equivalent to the ducted configuration, the 2D array needs to be infinitely large, although it can be approximated by a finite size array. Based on initial calculations, not included in this paper, it appears that the impedance is slow to converge and may require an array with hundreds of unit cells. Since the goal of this effort is to develop computationally efficient impedance models for variable depth samples, the numerical approach (i.e., create a large 2D array and then use Eqs. (8), (9), and (10) to solve for the radiation impedance of each resonator) was not pursued.

Nevertheless, the equivalent representation is still useful. For example, in Fig. 4(a), the sample consists of a single resonator located in the center of the duct. Fig. 4(b) shows a sample with a single resonator centered along one edge, and Fig. 4(c) shows a single resonator located in the corner. When the samples are mirrored and replicated, it is clear that the equivalent 2D arrays are different. In the first case, the equivalent representation consists of a periodic array of individual resonators equally spaced in the horizontal and vertical directions. The smallest unit cell that can be replicated and translated to create the larger array is 2" by 2" (i.e., the size of the duct). In the second case, groups of two resonators are lumped together and the smallest unit cell size is 4" by 2". In the third case, groups of four resonators are lumped together and the unit cell size is 4" by 4". While the open area ratio, σ, is the same for all three unit cells, the radiation impedance, as will be shown later in the paper, is different. The radiation loading on the resonator in the corner is much higher than the loading on the resonator in the center of the sample because of its proximity to the image sources. Recall from the previous section that the mutual interaction term is most important when resonators with the same natural frequency are located next to each other, which is essentially what happens when the resonators are placed along the edge, or in the corner of the sample.

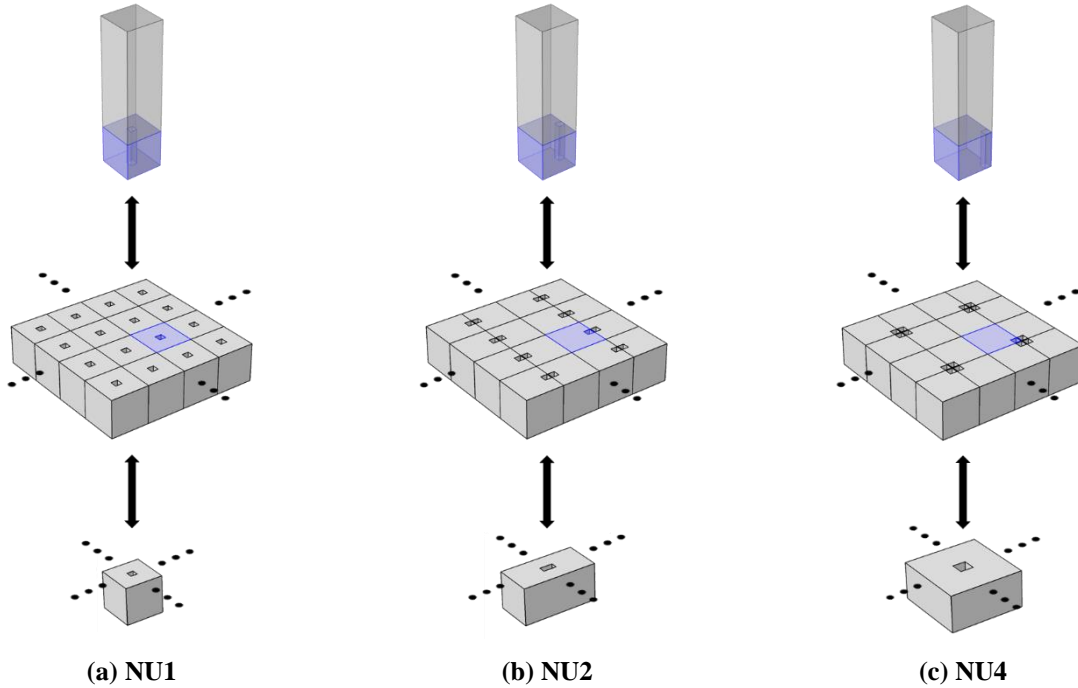**(a) NU1**   **(b) NU2**   **(c) NU4**

Fig. 4 The figures at the top depict the non-uniform sample installed in the end of a duct, the figures in the middle represent the equivalent two-dimensional resonator array, and the figures at the bottom represent the smallest periodic unit cell for that array.

C. End Corrections

Instead of explicitly solving Eq. (8), radiation loading is often approximated using a fictitious attached mass called an end correction. This approach is particularly well-suited for lumped parameter models and yields efficient impedance models suitable for use in optimization studies. Four different semi-analytical end corrections are considered next, starting with the end correction for a uniform array.

1. Plane wave (C1)

When uniform-depth resonators are configured in a dense 2D array, which is representative of conventional engine liners, a normally incident plane wave will excite the resonators equally. The particle velocity at each inlet will therefore be equal, and sound will radiate away from the array as a plane wave (as long as the separation distance between the resonators is sufficiently small with respect to the acoustic wavelength). The radiation impedance for a uniform array is therefore equal to the characteristic impedance of the medium (i.e., ρc). Since the imaginary component is zero, the mass loading, and therefore the end correction δ_{C1}, will also equal zero. The fact that the radiation reactance is zero means that the sum of the mutual impedance for all the resonators in the array completely cancels the self-radiation reactance. In other words, the interaction effect is very important, as one would expect for an array of closely spaced resonators tuned for the same frequency. When the sample is not uniform, the mass loading can be significant, as discussed below.

2. Baffled piston (C2)

An isolated resonator set in an infinite baffle represents an extreme example of a non-uniform "sample". If the resonator inlet is approximated by a mass-less piston, then the radiation impedance expression given in Eq. (9) can be used to define the end correction. Specifically, the normalized radiation reactance (i.e., imaginary part of the radiation impedance presented in Eq. (9) normalized by ρc) is

$$\chi_{C2} = k8r/3\pi \tag{11}$$

and the mass end correction is

$$\delta_{C2} = 8r/3\pi \tag{12}$$

In most cases, liner samples consist of more than one resonator, and the impedance is generally measured in an impedance tube, not an infinite baffle. As previously discussed, this changes the radiation impedance, and therefore the mass end correction.

3. Piston in a duct (C3)

The end correction for a single, center located resonator radiating into a duct, as shown in Fig. 4(a), can be estimated using a closed-form expression provided by Ref. [8],

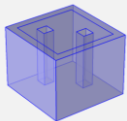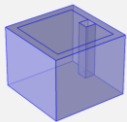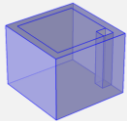$$\delta_{C3} = 8r/3\pi\left(1 - 1.25\sqrt{\sigma_i}\right) \tag{13}$$

where σ is the ratio of the inlet area of the resonator to the total surface area of the sample. This approximation is valid for $\sqrt{\sigma} < 0.4$, and is appropriate for a single, centered resonator radiating into a duct.

4. Location based (C4)

Recall that the goal of the paper is to develop an efficient model for variable depth liners. So instead of attempting a rigorous derivation of end corrections for arbitrary resonator combinations, several assumptions will be made to make the problem more tractable. As previously mentioned, the mutual interaction is most important when the resonators have the same natural frequency and are located close together. Recall that both variable depth samples were arranged so that no two cavities with the same depth are adjacent to each other. Therefore it is assumed that the mutual radiation impedance is small relative to the self-radiation impedance. In other words, the mutual interaction between the resonators within the sample, even the ones tuned for the same frequency, is neglected.

The self-radiation impedance, however, has to be considered. While closed-form approximations are available for specific configurations (such as a piston radiating into an infinite half space or a piston centered in one end of a duct), these may not be applicable for all resonators in the sample. Previous observations regarding Fig. 4 suggest that the radiation loading will depend on the location of the resonator within the sample. For example, the radiation loading on the resonator in the corner is anticipated to be much higher than the loading on the resonator in the center of the sample due to its proximity to the image sources. Therefore, to capture the location effects, each resonator is lumped into one of the three categories based on its location in the 5 by 5 array. The nine resonators in the interior (away from the duct walls) are lumped together, as are the twelve along the edge of the sample (but not in the corner). Finally, the four resonators in the corners make up the last group. Each of these categories (interior, edge, and corner) is depicted in Fig. 4, along with the corresponding unit cell representation at the bottom of the figure. Notice that each unit cell contains a single resonator centered within the sample. Therefore Eq. (13) can be modified to determine the appropriate end correction for each case. While the open area ratio, σ, is constant in all three cases, the cross-sectional area of the three resonators is different. In the first case, the effective cross-sectional area, A', is equal to the actual area, A, of the resonator and the appropriate end correction is identical to Eq. (13). In the second case, the effective area is $A' = 2A$. Therefore the effective radius is $r' = \sqrt{2A/\pi} = \sqrt{2}r$ and the mass end correction becomes $\delta = \left(\sqrt{2}r\right)8/3\pi\left(1 - 1.25\sqrt{\sigma_i}\right)$. Similarly, in the third case the effective area is $A' = 4A$ and the effective radius is $r' = \sqrt{4A/\pi} = 2r$. The mass end correction is therefore $\delta = (2r)8/3\pi\left(1 - 1.25\sqrt{\sigma_i}\right)$. The three categories and end corrections are summarized in Table 2. Note that the square superimposed on the top surface of the samples simply indicates the perimeter of the duct.

Table 2 Location based end correction, C4.

Location	End Correction	Example
Interior	$\delta_{C4} = (r)8/3\pi\left(1 - 1.25\sqrt{\sigma_i}\right)$	
Edge	$\delta_{C4} = (\sqrt{2}r)8/3\pi\left(1 - 1.25\sqrt{\sigma_i}\right)$	
Corner	$\delta_{C4} = (2r)8/3\pi\left(1 - 1.25\sqrt{\sigma_i}\right)$	

IV.   Numerical Model

A three-dimensional finite element model was created for comparison purposes. Both the liner sample and impedance tube were modeled explicitly and point measurements, taken at the same locations as the microphones in the normal incidence tube, were processed to predict the specific acoustic impedance of the sample. The thermal and viscous losses within the resonator(s) were captured using the Zwikker and Kosten dissipation model described previously. The system response (i.e., acoustic pressure) was found by solving the Helmholtz equation subject to the appropriate boundary conditions. Specifically, the walls of the duct and liner were assumed to be acoustically rigid and the source plane (on the opposite end of the duct as the liner sample) was defined as a plane-wave source. The acoustic domain was meshed using free tetrahedral quadratic Lagrange elements and the maximum element size was at least eight times smaller than the acoustic wavelength at the highest frequency of interest. The acoustic response was found using a direct frequency domain solution from 500 Hz to 3000 Hz in 25 Hz increments. The solve times varied based on the liner sample, but an average run time for the variable depth samples on a standard laptop (i7-6820HQ processor with 16 GB RAM) was 0.6 seconds per frequency.

V.   Results

The purpose of the current study is to assess semi-analytical impedance models, developed for variable depth liners, which include end corrections to account for the radiation loading on the resonators. Models are assessed by comparing predictions with measurements collected in the NASA Langley Normal Incidence Tube. Comparisons are initially presented for a uniform depth liner sample, followed by several non-uniform samples used to systematically evaluate candidate end corrections. Finally, two variable depth liner samples are considered.

A. Uniform Depth Sample

Measurements and predictions for a uniform liner sample are shown in Fig. 5. Specifically, the figure compares the normalized specific acoustic resistance and reactance spectra. Since the sample is uniform, predictions were generated using the semi-analytical impedance model with the C1 end correction, which means the radiation reactance was set to zero. The sample consists of 25 rectangular cavities that are each 1.505" deep. Since the depth is constant, the resonators all have the same natural frequency of approximately 2240 Hz, which can be identified by the zero crossing of the reactance. As the figure shows, the predictions closely match the measured reactance, which is dominated by the $-\cot(kh)$ behavior. The prediction misses the increase in resistance near 1900 Hz, but otherwise captures the measured trends.

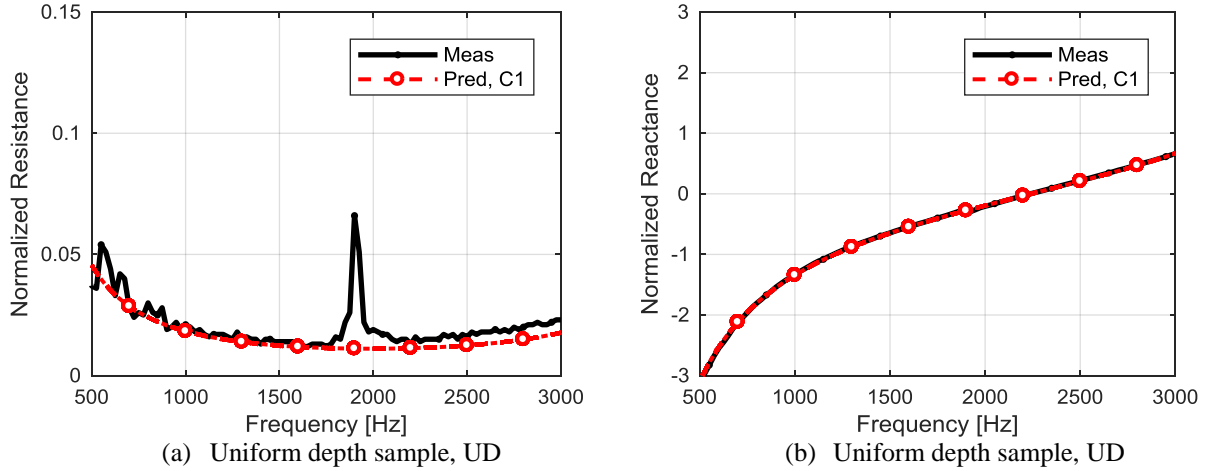(a) Uniform depth sample, UD

(b) Uniform depth sample, UD

Fig. 5 Predicted and measured normalized impedance spectra for the uniform depth sample. Predicted spectra were calculated using the C1 (plane wave) end correction.

B. Non-Uniform Samples

Normalized impedance spectra for two non-uniform samples are considered next. Specifically, Fig. 6 shows the measured impedance spectra for NU1 and NU4. Each sample contains a single resonator located either in the center or in the corner of the array. The scale on resistance is ten times larger than Fig. 5 to accommodate the higher resistance caused by the low open area ratio. In addition, the frequency range on the plots has been compressed relative to Fig. 5 to better identify the zero crossings of the reactance. The resonators are both 1.75" deep, which means the cavity resonance (i.e., one-quarter wave resonance) should be 1930 Hz. However, the zero crossings of the reactance are closer to 1800 Hz (for NU1) and 1700 Hz (for NU4). The shift relative to the one-quarter wave resonance, and also relative to each other, suggests that radiation loading is important and varies based on the location of the resonator in the sample. While the position of the resonator has a significant impact on reactance, the measured change in resistance is small. Therefore, subsequent plots will focus exclusively on reactance.
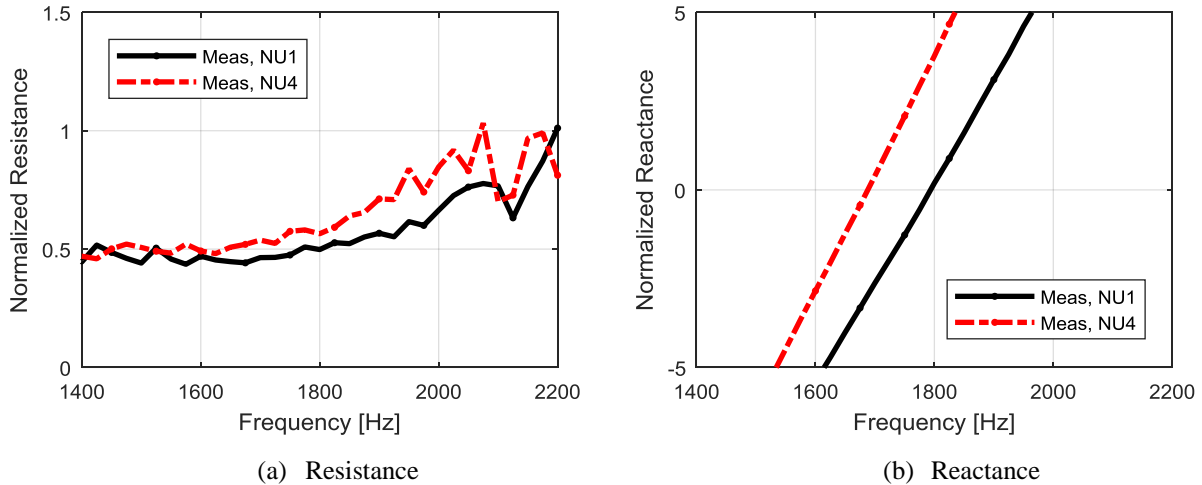

(a) Resistance

(b) Reactance

Fig. 6 Measured normalized impedance spectra for two non-uniform samples; NU1 and NU4.

Fig. 7 compares the measured reactance spectra for NU1 and NU4 with predictions generated using three different semi-analytical models. The first set of predictions was generated using end correction C1, which means the radiation reactance is set to zero. Recall that this approach accurately predicted the reactance for the uniform depth sample shown in Fig. 5(b). However, for the non-uniform samples considered here, the predicted reactance spectra is shifted to the right of the measured spectra by 100 Hz for NU1 and 200 Hz for NU4. The second set of predictions was generated using the C2 end correction. In this case, the radiation reactance is defined based on a piston radiating into an infinite half space. This model under predicts the natural frequency of NU1 by about 40 Hz and over predicts the

10

natural frequency of NU4 by 70 Hz. The third set of predictions was generated using C3, which captures the radiation reactance of a single center-located piston radiating into a duct. As expected, the prediction closely matches measurements for NU1, which consists of a single resonator located in the center of the sample. The comparison with NU4, however, is not as good. Predictions and measurements are offset by about 100 Hz.

(a) Non-uniform sample, NU1   (b) Non-uniform sample, NU4
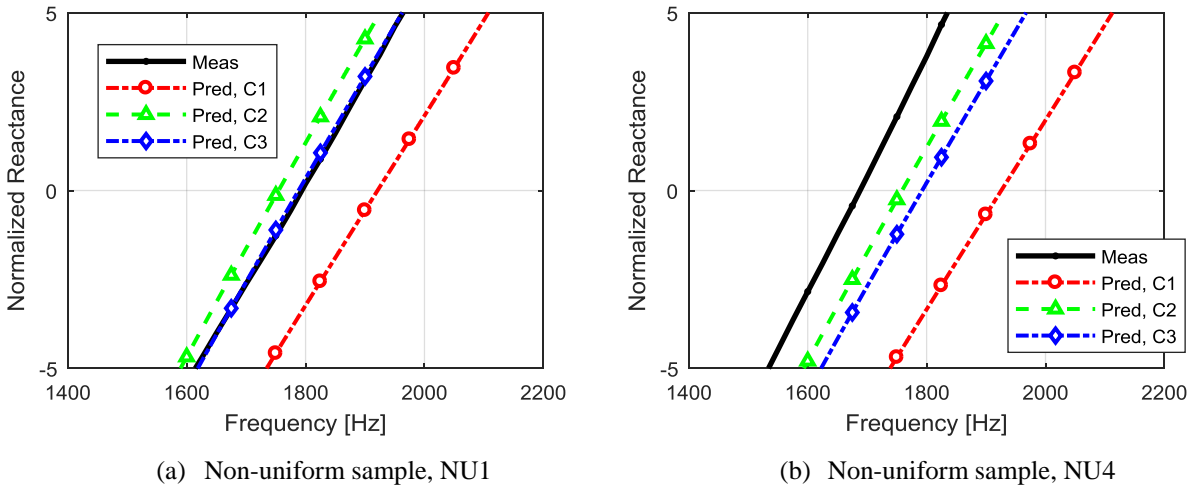
Fig. 7 Predicted and measured normalized reactance spectra for two non-uniform samples; NU1 and NU4. Predicted spectra were calculated using three different end corrections; C1 (plane wave), C2 (baffled piston), and C3 (piston in a duct).

The previous comparison demonstrated that C3 is appropriate for a single resonator located in the center of the sample, but does not capture the additional shift in the measured reactance observed when the resonator is located in the corner of the sample. To determine if C3 is appropriate for other resonator positions within the sample, predictions are compared with measured reactance spectra for NU3 and NU6 in Fig. 8. The first sample, NU3, contains a single resonator offset from the center of the array, and the second sample, NU6, contains two non-adjacent resonators within the interior of the array. Once again, the resonators are 1.75" deep and therefore the one-quarter wave resonance is 1930 Hz. While the natural frequency of both samples is approximately 1800 Hz, the slope of the reactance curve is shallower in Fig. 8(b) since the sample contains two resonators instead of one. The predicted spectra matches the measurements reasonably well in both cases. This implies that C3 may be an acceptable correction for resonators in the interior of the array. The favorable comparison observed in Fig. 8(b) also supports the hypothesis that the mutual interaction between resonators with the same length can be neglected when they are not adjacent to each other.

(a) Non-uniform sample, NU3   (b) Non-uniform sample, NU6
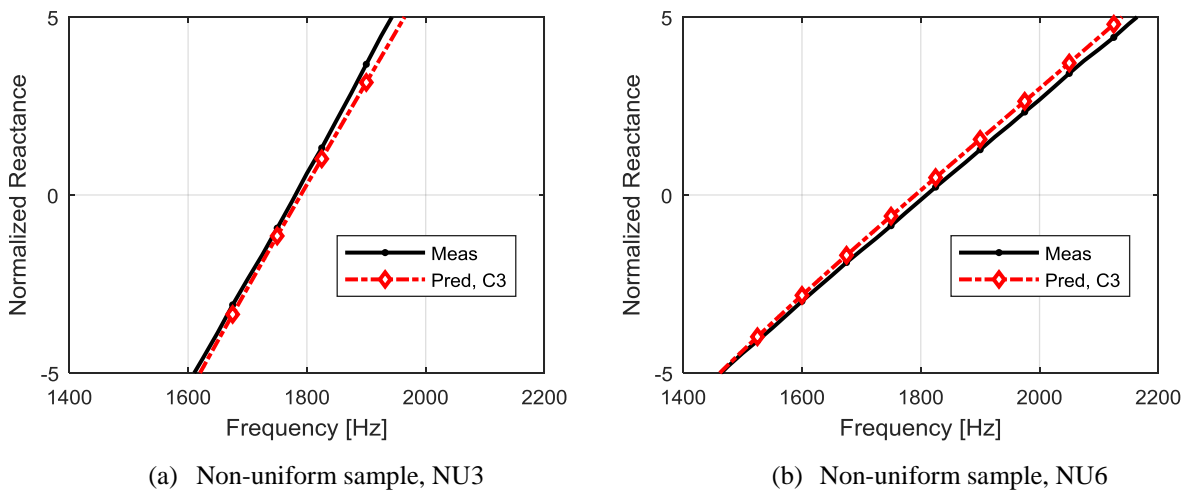
Fig. 8 Predicted and measured normalized reactance spectra for two non-uniform samples; NU3 and NU6. Predicted spectra were calculated using the C3 (piston in a duct) end correction.

11

The location based end correction, C4, is assessed next. Recall that in this case, different end corrections are used based on the location of the resonator within the array. As previously shown, the C3 end correction is appropriate for interior positions. Therefore, Fig. 9 compares measured and predicted reactance spectra for samples with resonators located along the edge (NU2), in the corner (NU4), and in both the corner and center of the array (NU5). The position based end corrections defined in Table 2 are used to generate the predictions. The predicted spectra match the measured reactance for all three samples. This is a promising result and suggests that a location based correction might be applicable for more complicated variable depth liner samples.

(a) Non-uniform sample, NU2   (b) Non-uniform sample, NU4   (c) Non-uniform sample, NU5
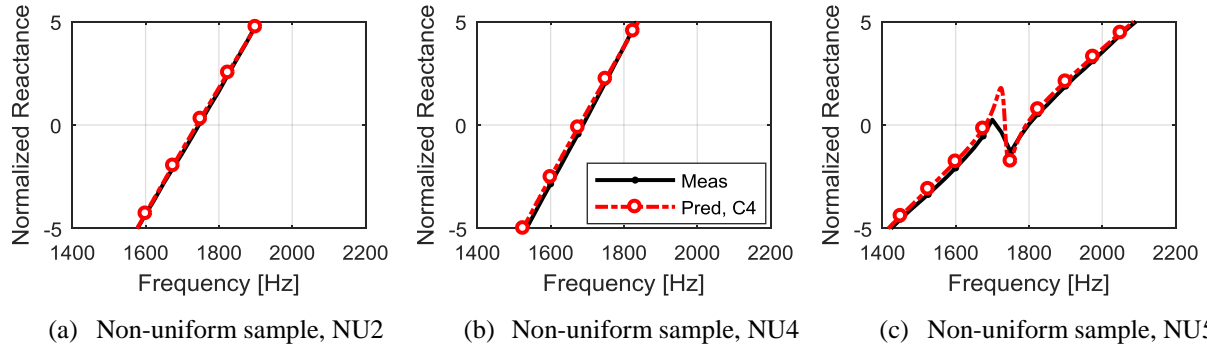
Fig. 9 Predicted and measured normalized reactance spectra for three non-uniform samples; NU2, NU4, and NU5. Predicted spectra were calculated using the C4 (location based) end correction.

C. Variable Depth Samples

Recall that two different variable depth samples were tested. The first sample, VD1, contains 7 unique depths and the second, VD2, contains 11 unique depths with one-quarter wave resonance frequencies from approximately 1000 Hz to 3000 Hz. Initially, predictions are generated with the C1 end correction, which neglects the radiation reactance. Once again, recall that predictions generated using this model closely matched measurements acquired with the uniform depth sample. The comparison for the variable depth samples is shown in Fig. 10. In this case, the predicted spectra is shifted to the right, relative to the measurements, particularly at high frequencies. It appears that the radiation loading, which was neglected in this case, is important for variable depth samples.

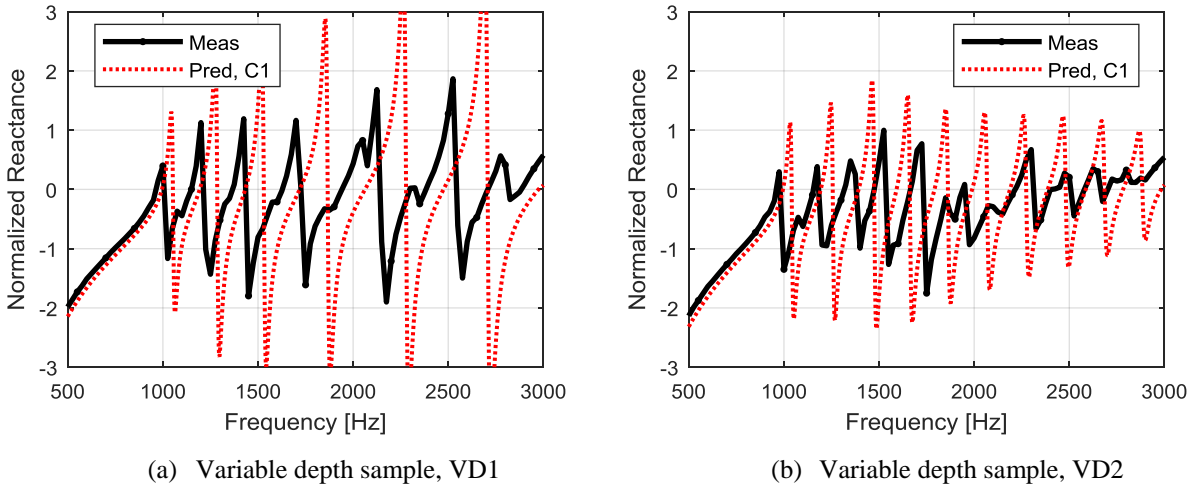(a) Variable depth sample, VD1   (b) Variable depth sample, VD2

Fig. 10 Predicted and measured normalized reactance spectra for the variable depth samples. Predicted spectra were calculated using the C1 (plane wave) end correction.

The location based end correction, C4, is considered next. Previous comparisons showed that this approach captured the change in the radiation loading based on the position of the resonator in the array. Fig. 11 shows the corresponding predicted and measured reactance spectra for both variable depth samples. The level of agreement is much better than previously observed in Fig. 10. The peaks and troughs are generally aligned, although the match is not perfect. The predictions appear to be shifted slightly to the left relative to the measurements and there are a few

extra peaks and troughs in the predicted spectra above 1500 Hz that do not align with the measurements. Recall however, that the prediction lumps all resonators into one of three categories based on location, and completely neglects the mutual radiation impedance between resonators. So some differences are expected. Nevertheless, the agreement is likely sufficient for early design purposes.

(a) Variable-depth sample, VD1   (b) Variable-depth sample, VD2
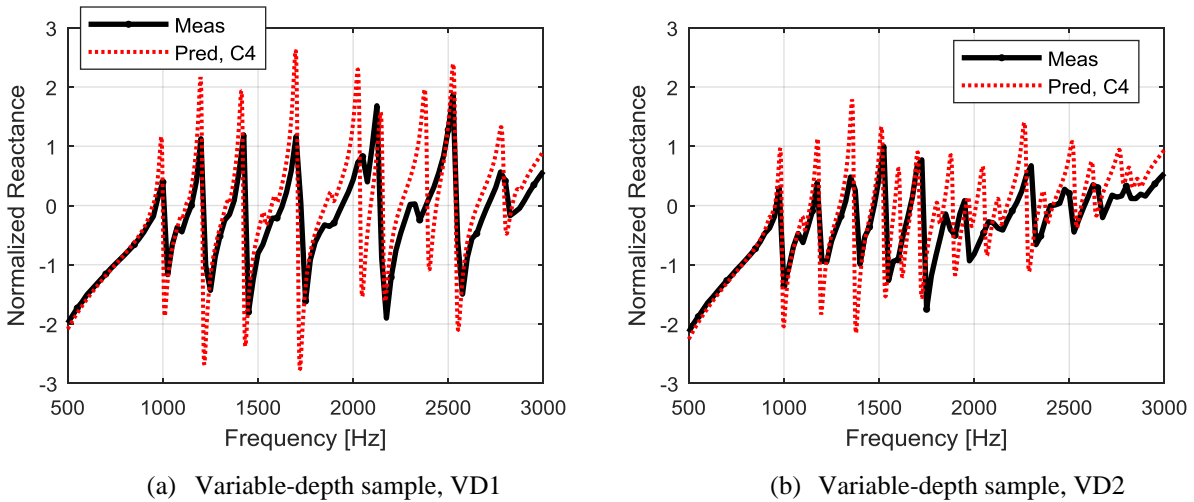
Fig. 11 Predicted and measured normalized reactance spectra for the variable depth samples. Predicted spectra were calculated using the C4 (location based) end correction.

Finally, finite element predictions are compared with measurements in Fig. 12. Notice that the finite element model accurately captures the interaction between the resonators in the variable depth samples, including detailed variations in the reactance spectra. The radiation loading is captured by default using this type of model since the resonators and impedance tube are explicitly modeled. Note that the finite element models takes considerably longer to run, however, than the semi-analytical model. The solve time for the finite element model on a standard laptop is approximately 0.6 seconds per frequency, or 60 seconds for the impedance spectra shown in Fig. 12. The semi-analytical model, in comparison, is more than 3 orders of magnitude faster. So, while the semi-analytical model may be a more appropriate objective function in an optimization study, the finite element model provides an attractive alternative when accuracy is more important than computational efficiency.

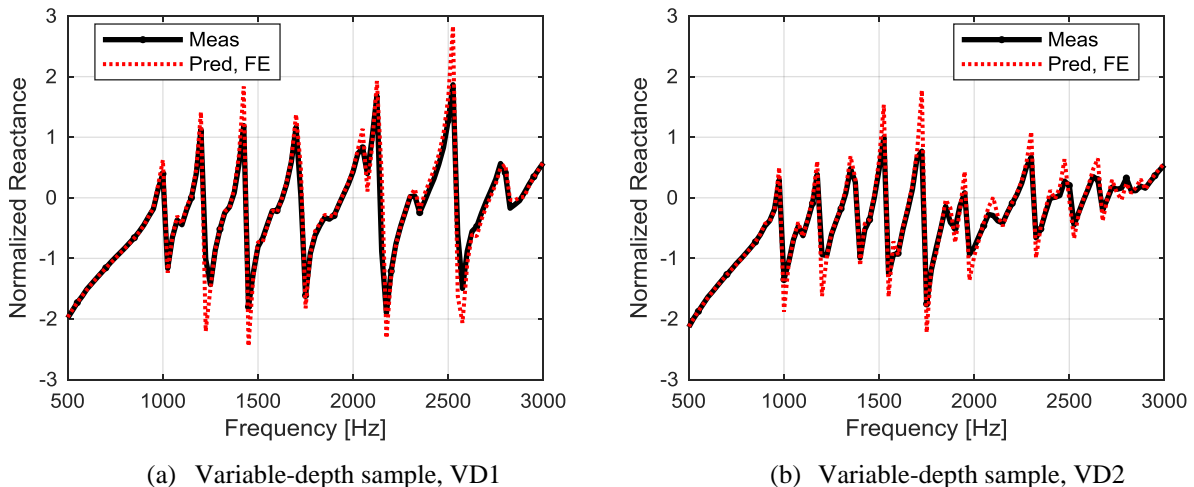(a) Variable-depth sample, VD1   (b) Variable-depth sample, VD2

Fig. 12 Predicted and measured normalized reactance spectra for the variable depth samples. Predicted spectra were generated using the finite element model.

VI.   Concluding Remarks

The purpose of this study was to assess smeared impedance models for variable depth liners consisting of groups of resonators tuned for different frequencies. When the array of resonators is not uniform, the radiation loading on each resonator can be significant, shifting the system resonances to lower frequencies. In contrast, when the liner consists of a dense array of uniform resonators, the radiation loading is negligible and a classical smeared impedance model can be used to accurately predict impedance. Tests performed on sparsely populated resonator samples confirmed that the radiation loading can be approximated using relatively simple end correction terms. An impedance model incorporating the proposed end corrections was evaluated by comparing predictions with measurements acquired on variable depth samples. The predicted and measured spectra agreed reasonably well, particularly given the simplicity of the model. Additional findings are listed below:

- The radiation loading on individual resonators in a non-uniform array can be significant and can vary based on the location of the resonator in the array.
- The mutual radiation impedance between pairs of resonators can typically be neglected, unless the resonators are tuned for the same frequency and are adjacent to each other.
- A relatively simple end correction, proposed by Ingard, can be modified to account for the radiation loading on resonators in sparsely populated arrays.
- Predictions generated using a simplified impedance model agree reasonably well with normal incidence tube measurements collected on variable depth liner samples.
- A finite element model can accurately predict the smeared impedance of variable depth liner samples, providing an alternative to semi-analytical models when accuracy is more important than computational efficiency.

In summary, this study demonstrated that semi-analytical impedance models can be used to predict the smeared impedance of variable depth liners. These models could, therefore, be used within an optimization to design broadband acoustic liners.

Acknowledgments

References

[1]Parrott, T. L., and Jones, M. G., "Parallel-element liner impedances for improved absorption of broadband sound in ducts," *Noise Control Engineering Journal*, Vol. 43, No. 6, 1995.

[2]Jones, M. G., Howerton, B. M., and Ayle, E., "Evaluation of Parallel-Element, Variable-Impedance, Broadband Acoustic Liner Concepts," AIAA Paper 2012-2194, June 2012.

[3]ISO 10534-2, Acoustics – Determination of Sound Absorption Coefficient and Impedance in Impedance Tubes, Part 2: Transfer-Function Method, ISO, Report No. ISO 10534-2:1998(E), 1998.

[4]Zwikker, C., and Kosten, C.W., *Sound Absorbing Materials*, Elsevier, Amsterdam, 1949.

[5]Tijdeman, H., "On the propagation of sound waves in cylindrical tubes," *Journal of Sound and Vibration*, Vol. 39, No. 1, 1975.

[6]Pritchard, R. L., "Mutual Acoustic Impedance between Radiators in an Infinite Rigid Plane," *Journal of the Acoustical Society of America*, Vol. 32, No. 6, 1960.

[7]Pierce, A. D., *Acoustics: An Introduction to its Physical Principles and Applications*, Acoustical Society of America, Melville, New York, 1989.

[8]Ingard, U., "On the Theory and Design of Acoustic Resonators," *Journal of the Acoustical Society of America*, Vol. 25, No. 6, 1953.